Anal. Chem. **2007,** *79,* 4484−4492

Laser-Induced Mixing in Microfluidic Channels

Amy N. Hellman,[†,‡,§] Kaustubh R. Rau,[†,‡,∥,⊥] Helen H. Yoon,[#] Stephanie Bae,[†] James F. Palmer,[¶] K. Scott Phillips,[¶] Nancy L. Allbritton,[¶,#] and Vasan Venugopalan*[,†,‡,∥]

Department of Biomedical Engineering, Department of Chemical Engineering and Materials Science, Department of Chemistry, Laser Microbeam and Medical Program, Beckman Laser Institute, and Department of Physiology and Biophysics, University of California, Irvine, Irvine, California 92697, and Department of Bioengineering, University of California, San Diego, La Jolla, California 92093

We demonstrate a novel strategy for mixing solutions and initiating chemical reactions in microfluidic systems. This method utilizes highly focused nanosecond laser pulses from a Q-switched Nd:YAG laser at $\lambda = 532$ nm to generate cavitation bubbles within 100- and 200-μm-wide microfluidic channels containing the parallel laminar flow of two fluids. The bubble expansion and subsequent collapse within the channel disrupts the laminar flow of the parallel fluid streams and produces a localized region of mixed fluid. We use time-resolved imaging and fluorescence detection methods to visualize the mixing process and to estimate both the volume of mixed fluid and the time scale for the re-establishment of laminar flow. The results show that mixing is initiated by liquid jets that form upon cavitation bubble collapse and occurs ~20 μs following the delivery of the laser pulse. The images also reveal that mixing occurs on the millisecond time scale and that laminar flow is re-established on a 50-ms time scale. This process results in a locally mixed fluid volume in the range of 0.5−1.5 nL that is convected downstream with the main flow in the microchannel. We demonstrate the use of this mixing technique by initiating the horseradish peroxidase-catalyzed reaction between hydrogen peroxide and nonfluorescent *N*-acetyl-3,7-dihydroxyphenoxazine (Amplex Red) to yield fluorescent resorufin. This approach to generate the mixing of adjacent fluids may prove advantageous in many microfluidic applications as it requires neither tailored channel geometries nor the fabrication of specialized on-chip instrumentation.

The challenge of rapidly mixing two fluids within a laminar flow has received considerable attention within the microfluidics community.[1−7] Microfluidic devices possess characteristic channel widths in the range $W \sim 50-500$ μm with volumetric flow rates of $Q \sim 50-500$ μL/h resulting in Reynolds numbers of $Re \ll 10$. The resulting laminar flow admits only diffusion as a mechanism to mix two adjacent fluid streams. The reliance on diffusion alone for the mixing of reactants results in extremely long mixing times and lengths. Specifically, molecular diffusion across a distance of 100 μm requires times of 10−1000 s when considering molecules with diffusivities in the range of $10^{-3}-10^{-5}$ mm^2/s.[8] This translates into mixing lengths of 0.1−10 m. Such mixing times and lengths are clearly impractical for rapid mixing of small volumes. Thus microfluidic devices that aim to provide rapid kinetic biochemical analysis cannot rely on diffusion alone to mix reagents. Several articles have considered in detail these issues pertaining to flow and transport at the microscale.[8−11]

The limitations posed by diffusion-based transport have spurred researchers to develop various strategies to rapidly mix small volumes in microfluidic devices. Generally these strategies either employ changes in channel geometry (static mixers) or introduce external energy sources (active mixers) to enhance fluid contact or destabilize the laminar flow.[12] In static mixers, the simplest design modifications are to increase channel length and tortuosity to increase fluid contact time and enhance diffusion. The use of hydrodynamic focusing to achieve reductions in both the flow cross section and molecular diffusion time has also been described.[13−15] Such hydrodynamic focusing strategies have

* To whom correspondence should be addressed. Phone: (949) 824-5802. Fax: (949) 824-2541. E-mail: vvenugop@uci.edu.

† Department of Chemical Engineering and Materials Science, University of California, Irvine.

‡ Laser Microbeam and Medical Program, Beckman Laser Institute, University of California, Irvine.

§ Department of Bioengineering, University of California, San Diego.

∥ Department of Biomedical Engineering, University of California, Irvine.

⊥ Current address: National Centre for Biological Sciences, Tata Institute of Fundamental Research, Bangalore 560 065, India.

Department of Chemistry, University of California, Irvine.

¶ Department of Physiology and Biophysics, University of California, Irvine.

(1) He, B.; Burke, B. J.; Zhang, X.; Regnier, F. E. *Anal. Chem.* **2001**, *73*, 1942−1947.
(2) Jacobson, S. C.; McKnight, T. E.; Ramsey, J. M. *Anal. Chem.* **1999**, *71*, 4455−4459.
(3) Liau, A.; Karnik, R.; Majumdar, A.; Cate, J. H. D. *Anal. Chem.* **2005**, *77*, 7618−7625.
(4) Johnson, T. J.; Ross, D.; Locascio, L. E. *Anal. Chem.* **2002**, *74*, 45−51.
(5) Park, H. Y.; Qiu, X. Y.; Rhoades, E.; Korlach, J.; Kwok, L. W.; Zipfel, W. R.; Webb, W. W.; Pollack, L. *Anal. Chem.* **2006**, *78*, 4465−4473.
(6) Seong, G. H.; Crooks, R. M. *J. Am. Chem. Soc.* **2002**, *124*, 13360−13361.
(7) Gartecki, P.; Fuerstman, M. J.; Fischbach, M. A.; Sia, S. K.; Whitesides, G. M. *Lab Chip* **2006**, *6*, 207−212.
(8) Ottino, J. M.; Wiggins, S. *Philos. Trans. R. Soc. London, A* **2004**, *362*, 923−935.
(9) Squires, T. M.; Quake, S. R. *Rev. Mod. Phys.* **2005**, *77*, 977−1026.
(10) Ho, C. M.; Tai, Y. C. *Annu. Rev. Fluid Mech.s* **1998**, *30*, 579−612.
(11) Papautsky, I.; Brazell, J.; Ameel, T.; Frazier, A. B. *Sens. Actuators, A* **1999**, *73*, 101−108.
(12) Campbell, C. J.; Gryzbowski, B. A. *Philos. Trans. R. Soc. London, A* **2004**, *362*, 1069−1086.
(13) Knight, J. B.; Vishwanath, A.; Brody, J. P.; Austin, R. H. *Phys. Rev. Lett.* **1998**, *80*, 3863−3866.

10.1021/ac070081i CCC: $37.00
Published on Web 05/18/2007

provided mixing times as rapid as 8 μs.[16] In other areas, researchers have designed static mixers that utilize chaotic advection, a process in which fluid interfaces undergo stretching and folding to achieve higher mixing efficiencies. Mixers that employ chaotic advection can involve complex designs with three-dimensional microchannels or relief features on the microchannel floor to achieve mixing of two fluid streams.[17−19] In active mixers, an energy source is used to destabilize the laminar flow. A simple case of this approach utilizes the temporal pulsing of the flow rate of two fluid streams and has been shown to create well-mixed regions within 250 ms in a 200 μm × 120 μm channel at a flow rate of 1.55 μL/s.[20] Designs employing ultrasound,[21,22] electroosmotic flow,[23] dielectrophoresis,[24] and magnetic microstirrers[25,26] have all been examined to mix two fluids within microchannels. Thus, a multitude of approaches have been proposed to handle the microfluidic mixing problem. The choice of mixer type is best determined by the specific application and other considerations such as complexity of design and fabrication.

In this report, we present a new method to provide rapid, localized mixing of fluids in microfluidic channels on demand. The concept utilizes the delivery of a highly focused nanosecond laser pulse resulting in plasma formation and subsequent cavitation bubble generation. The three-dimensional character of the fluid flow associated with the cavitation dynamics causes two adjacent fluid streams to mix on microsecond to millisecond time scales. This laser-based method of fluid mixing has several important characteristics that distinguish it from those using more conventional active mixing methods such as ultrasound. First, laser-generated cavitation produces a volume of mixed fluid only in the region surrounding the laser focal volume, thereby enabling the production of a locally mixed fluid volume within the microfluidic channel. Second, the focal volume of the laser beam can be moved easily, and thus, the site of mixing is not fixed at a particular location in the device. Third, the laser delivery can be easily switched on and off to provide fluid mixing only at specific times in a microfluidic process. Last, since the laser is decoupled from the microfluidic device, this approach provides microfluidic mixing capabilities without requiring any modification to the microfluidic device design or fabrication. Pulsed laser microbeams also offer additional capabilities in a microfluidic context and can provide a multifunctional tool for capabilities such as selective cell lysis,[27] fluorescence excitation, and uncaging of photoexcitable compounds.[28] Finally, one can envision new applications wherein the use of an on-demand, localized mixing capability could prove useful, for example, to mix small volumes of two reactants to synthesize small quantities of product.

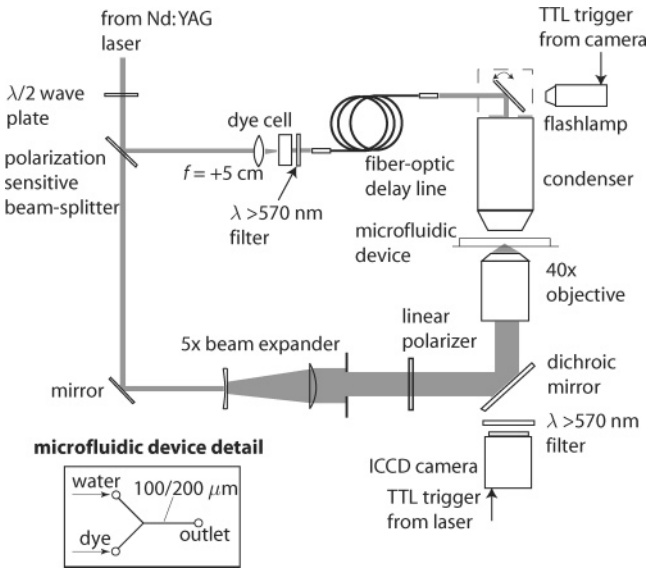

Figure 1. Setup for laser-induced mixing and time-resolved imaging.

In this study, a highly focused Q-switched Nd:YAG laser emitting 6-ns duration pulses at λ = 532 nm was used to produce mixing within the parallel flow of two adjacent fluids within a microfluidic channel. The dynamics and extent of mixing were assessed in three studies. First, time-resolved photography was used to visualize the spatiotemporal dynamics of the cavitation-induced mixing at the site of laser pulse delivery on nanosecond to millisecond time scales. Second, a fluorescence detection system was used to examine the spatial extent of the mixed bolus of fluid ~7 mm downstream from the site of pulsed laser delivery. Third, fluorescence video microscopy was used to visualize the efficacy of this mixing approach to initiate a biochemical reaction. This was done by establishing the parallel flow of two adjacent fluid streams containing nonfluorescent substrate and catalyst molecules that, when mixed, yield a fluorescent product.

MATERIALS AND METHODS

Microfluidic Device. The microfluidic device was fabricated from poly(dimethylsiloxane) (PDMS) using casting techniques. A SU-8 photoresist layer was spin coated onto a silicon wafer, and the desired pattern was etched using standard photolithography techniques. The channel design (shown in the lower left-hand corner of Figure 1) consisted of two inlets and an outlet in the form of a Y, with channel widths of either 100 or 200 μm and a channel depth of 50 μm. Two-part silicone resin (Sylgard 184, Dow Corning Corp.) was mixed in a 10:1 ratio (part A/part B, v/v), poured over the silicon master, degassed, and cured at 70 °C for 1 h. The cured polymer was peeled from the silicon wafer and

(14) Shapiro, H. M. *Practical flow cytometry,* 4th ed.; Wiley-Liss: New York, 2003.
(15) Spielman, L.; Goren, S. L. *J. Colloid Interface Sci.* **1968**, *26*, 175−182.
(16) Hertzog, D. E.; Michalet, X.; Jager, M.; Kong, X.; Santiago, J. G.; Weiss, S.; Bakajin, O. *Anal. Chem.* **2004**, *76*, 7169−7178.
(17) Liu, R. H.; Stremler, M. A.; Sharp, K. V.; Olsen, M. G.; Santiago, J. G.; Adrian, R. J.; Aref, H.; Beebe, D. J. *J. Microelectromech. Syst.* **2000**, *9*, 190-197.
(18) Therriault, D.; White, S. R.; Lewis, J. A. *Nat. Mater.* **2003**, *2*, 265−271.
(19) Stroock, A. D.; Dertinger, S. K. W.; Ajdari, A.; Mezić, I.; Stone, H. A.; Whitesides, G. M. *Science* **2002**, *295*, 647−651.
(20) Glasgow, I.; Aubry, N. *Lab Chip* **2003**, *3*, 114−120.
(21) Liu, R. H.; Yang, J.; Pindera, M. Z.; Athavale, M.; Grodzinski, P. *Lab Chip* **2002**, *2*, 151−157.
(22) Yaralioglu, G. G.; Wygant, I. O.; Marentis, T. C.; Khuri-Yakub, B. T. *Anal. Chem.* **2004**, *76*, 3694−3698.
(23) . Oddy, M. H.; Santiago, J. G.; Mikkelsen, J. C. *Anal. Chem.* **2001**, *73*, 5822−5832.
(24) Deval, J.; Tabeling, P.; Ho, C. M. *Proc. 15th IEEE Int. Conf. MEMS* **2002**, 36−39.
(25) Lu, L. H.; Ryu, K. S.; Liu, C. *J. Microelectromech. Syst.* **2002**, *11*, 462−469.
(26) Suzuki, H.; Kasagi, N.; Ho, C. M. *Proc. 3rd Int. Symp. Turbulence Shear Flow Phenomema* **2003**, 817−822.
(27) Krasieva, T. B.; Chapman, C. F.; Lamorte, V. J.; Venugopalan, V.; Berns, M. W.; Tromberg, B. J. *Proc. SPIE* **1998**, *3260*, 38−44.
(28) Paul, P. H.; Garguilo, M. G.; Rakestraw, D. J. *Anal. Chem.* **1998**, *70*, 2459−2467.

sealed against a glass coverslip after punching inlet and outlet vias for fluid access.

Time-Resolved Bright-Field Imaging of Laser-Induced Mixing. Figure 1 is a schematic of the experimental system used in the time-resolved imaging experiments. Fluid was metered into the microfluidic channels using two 100-μL syringes (Gastight No. 81026, Hamilton Co.) that were connected to the device using Teflon tubing and driven by a syringe pump (Pump 11, Harvard Apparatus). Two fluid streams consisting of water and 8 mg/mL Naphthol Green dye (Sigma), respectively, were supplied from separate syringes each at a flow rate of 50 μL/h into individual channels of 100- or 200-μm width. The total flow rate of 100 μL/h resulted in mean flow velocities of 2.8 and 5.6 mm/s in channels of 200- and 100-μm width, respectively.

The microfluidic device was placed on the sample stage of an inverted microscope (Zeiss Axiovert A110), and the $\lambda = 532$ nm output from a frequency-doubled Q-switched Nd:YAG laser (INDI I-10, Spectra Physics) with a pulse duration of $t_p = 6$ ns was introduced through the fluorescence port into the rear aperture of a microscope objective (Zeiss Acroplan 40×, 0.8 NA or 20×, 0.5 NA). The focal volume of the objective was positioned within the microfluidic channel at the interface between the two parallel fluid streams. Laser pulse energies in the range of 20−25 μJ were employed in all the experiments reported. The laser pulse generated a plasma on the nanosecond time scale resulting in the formation of a cavitation bubble that, upon collapse, produced mixing of the adjacent fluid streams. Mixing dynamics were visualized using a custom-built, time-resolved imaging setup that has been described previously[29,30] and employs the emission from a fluorescent dye cell or an ultrashort duration flashlamp to provide image illumination to the microscope condenser at the desired delay time. A gated intensified CCD camera (PI-MAX, Roper Scientific) was mounted on the microscope for image capture. The camera gate duration was set to 0.5 ns when using the fluorescent dye cell for illumination and 200 ns when using the flashlamp illumination due to electronic jitter in the flashlamp triggering. Thus, when using the flashlamp illumination, i.e., for time delays longer than 3.6 μs, the exposure duration was governed by the 40-ns duration of the flash lamp. WinView software (Roper Scientific) was used to control relevant image acquisition parameters such as gate delay and gate duration as well as coordinating the delivery of the pulsed laser radiation and the image illumination. Differential transmission of the illumination pulse through the water and dye streams generated contrast and allowed these dynamics to be imaged.[17] Adjustments to image brightness and contrast were performed subsequently using Adobe Photoshop (Adobe Systems, Cupertino, CA) as necessary. Each time point was imaged a minimum of three times and representative images are shown in Results and Analysis.

Fluorescence System for Downstream Detection of Mixed Dynamics. To examine the dynamics downstream from the site of laser delivery, we utilized the same microfluidic configuration described above but replaced the Naphthol Green dye solution with a solution of 10 μM fluorescein and employed a fluorescence detection system, as shown in Figure 2. The two fluids were pumped individually at a flow rate of 50 μL/h through a 200-μm-wide channel and brought together at a Y junction. To monitor the presence of fluorescent molecules within the channel, the output of a continuous-wave argon ion laser at $\lambda = 488$ nm (2214-10SL, JDS Uniphase) was coupled through a single-mode fiber optic and reflected by a dichroic mirror into the back aperture of a microscope objective (Nikon, 50×, 0.55 NA) that was screwed into a custom-made filter block. The objective directed the argon ion laser beam to the desired location within the microfluidic channel. Any fluorescent emission collected by the microscope objective was directed to a photomultiplier tube (PMT, R928, Hamamatsu Photonics) that was also attached to the filter block. A long-pass filter (LP 500, Edmund Scientific) was used to prevent any argon ion laser light from reaching the PMT, and a 50-μm-diameter pinhole was placed in front of the PMT to provide confocal detection. This assembly was mounted on a three-axis translation stage that was fixed to the microscope stage above the microfluidic device. The translation stage allowed positioning of the detection system at a defined distance downstream from the microscope objective that delivered the pulsed Nd:YAG laser radiation to produce mixing. Moreover, the translation stage provided precise positioning of the focal volume of the argon ion laser beam at the desired lateral and depth locations within the channel. The fluorescence excitation volume provided by the argon ion laser was positioned laterally on the "water side" of the channel 20 μm from the channel wall and 80 μm from the water fluorescein interface. This configuration ensured that fluorescence would not be detected when no mixing was accomplished and that appearance of a PMT signal indicated the presence of fluorescein throughout nearly the entire width of the microfluidic channel. The Nd:YAG laser was fired at a repetition rate of 0.4 Hz while the PMT monitored the fluorescence emission at 60 Hz. Custom software routines written in Testpoint (Keithley MetraByte) provided automated control over the delivery of Nd:YAG laser pulses and PMT signal collection.

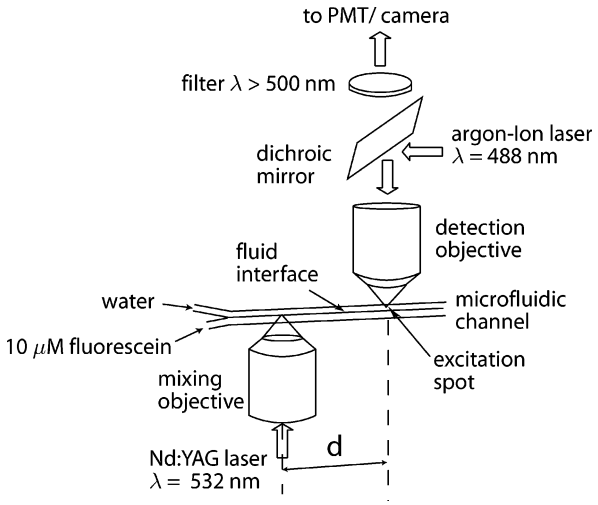

Figure 2. Setup for fluorescent system for downstream confocal detection of mixed fluid. The separation distance *d* between the site of mixing and the site of fluorescent detection is ~7 mm.

Fluorescence Detection of Amplex Red/Horseradish Peroxidase (HRP) Reaction. To demonstrate that the mixing provided by this technique can be utilized to initiate an enzyme-catalyzed biochemical reaction, we imaged the generation of

(29) Rau, K. R.; Guerra III, A.; Vogel, A.; Venugopalan, V. *Appl. Phys. Lett.* **2004**, *84*, 2940−2942.
(30) Rau, K. R.; Quinto-Su, P. A.; Hellman, A. N.; Venugopalan, V. *Biophys. J.* **2006**, *91*, 317−329.

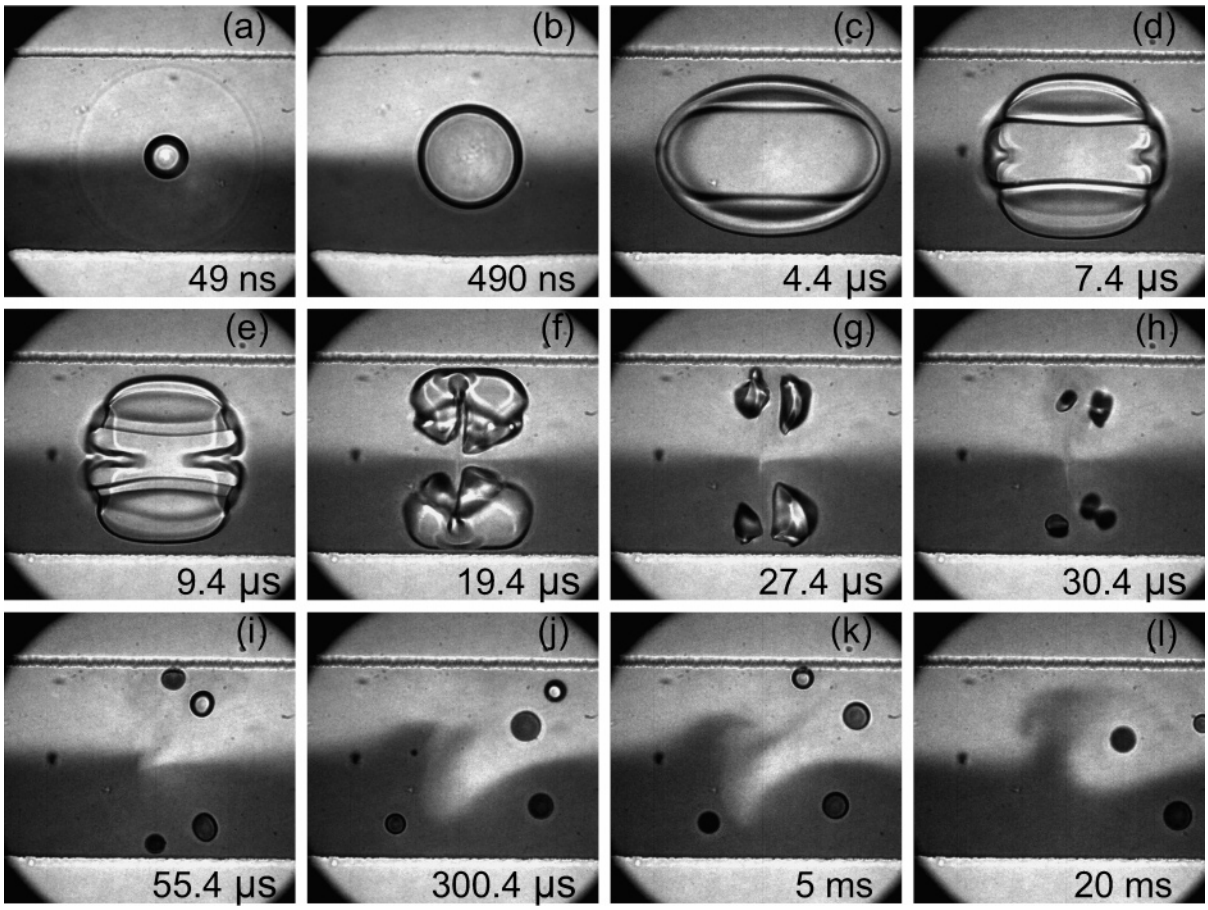

Figure 3. Time-resolved image series of cavitation bubble expansion and collapse and subsequent mixing effects produced by a single nanosecond laser pulse in a 200-μm-wide microfluidic channel.

fluorescent resorufin resulting from mixing two nonfluorescent reactant streams, one containing Amplex Red and the other containing HRP and hydrogen peroxide. The two fluids were pumped individually through 100-μm-wide channels and brought together at a Y junction. Amplex UltraRed reagent, HRP, and 1 M Tris-HCL buffer were acquired from Invitrogen Corp. (Carlsbad, CA). The 30% H_2O_2 and dimethyl sulfoxide (DMSO) were acquired from Sigma Chemical Co. (St. Louis, MO). All chemicals were reagent-grade quality or better. A 10 mM stock solution of Amplex Red was prepared in DMSO, and a 300 units/mL stock solution of HRP was made using 0.1 M Tris-HCL buffer solution. Immediately prior to use, the stock solutions were diluted in 0.1 M Tris-HCL buffer solution to make one solution containing 250 μM Amplex Red and one solution containing 160 μM H_2O_2 and 1.6 units/mL HRP. Each solution was metered using a 10-μL syringe (Gastight No. 1701, Hamilton Co.) connected to the device using Teflon tubing and driven by a syringe pump (Pump 11, Harvard Apparatus) at a flow rate setting of 5 μL/h into a 100-μm channel resulting in a mean flow velocity of 560 μm/s in the main channel.

Bright-field and fluorescence images of the enzyme reaction were acquired using the Zeiss Axiovert microscope described above equipped with a 100-W mercury lamp and band-pass filters (λ_{ex} = 540 nm, λ_{em} = 630 nm, Chroma Technology Corp.). The laser was fired to generate mixing, and the production of resorufin was imaged using a digital video camera (Panasonic GP-KR222) and saved using a video cassette recorder (JVC HR-S7800U). Still images at desired time points were captured from the taped recording using Power Director Pro 2.5ME software (CyberLink USA, Fremont, CA).

RESULTS AND ANALYSIS

Time-Resolved Bright-Field Imaging of Laser-Induced Mixing. Delivery of nanosecond Nd:YAG laser pulses focused within the microfluidic channel induced plasma formation in the fluid whose expansion resulted in shock wave emission and cavitation bubble formation. The plasma formation and shock wave dynamics have been well-studied,[29,31,32] and here we focus on the cavitation dynamics as it serves as the agent for the observed fluid mixing. Figure 3 provides images from our time-resolved photography apparatus depicting the shock wave propagation, cavitation bubble formation, expansion, and collapse at various time points following the delivery of a single 20-μJ laser pulse within the 200-μm channel. The time point is given in each frame, and the flow is from viewer's left to right. Figure 3a reveals a shock wave resulting from the rapid plasma expansion and cavitation bubble formation. The high pressure within the bubble causes its initial rapid expansion that begins to slow measurably on a time scale of $\lesssim$100 ns.[33] The bubble assumes an ellipsoidal shape as its expansion is constrained by the channel walls (Figure 3c).

(31) Venugopalan, V.; Guerra III, A.; Nahen, K.; Vogel, A. *Phys. Rev. Lett.* **2002**, *88*, 078103.
(32) Vogel, A.; Nahen, K.; Theisen, D.; Noack, J. *IEEE J. Sel. Top. Quantum Electron.* **1996**, *2*, 847−860.
(33) Vogel, A.; Busch, S.; Parlitz, U. *J. Acoust. Soc. Am.* **1996**, *100*, 148−165.

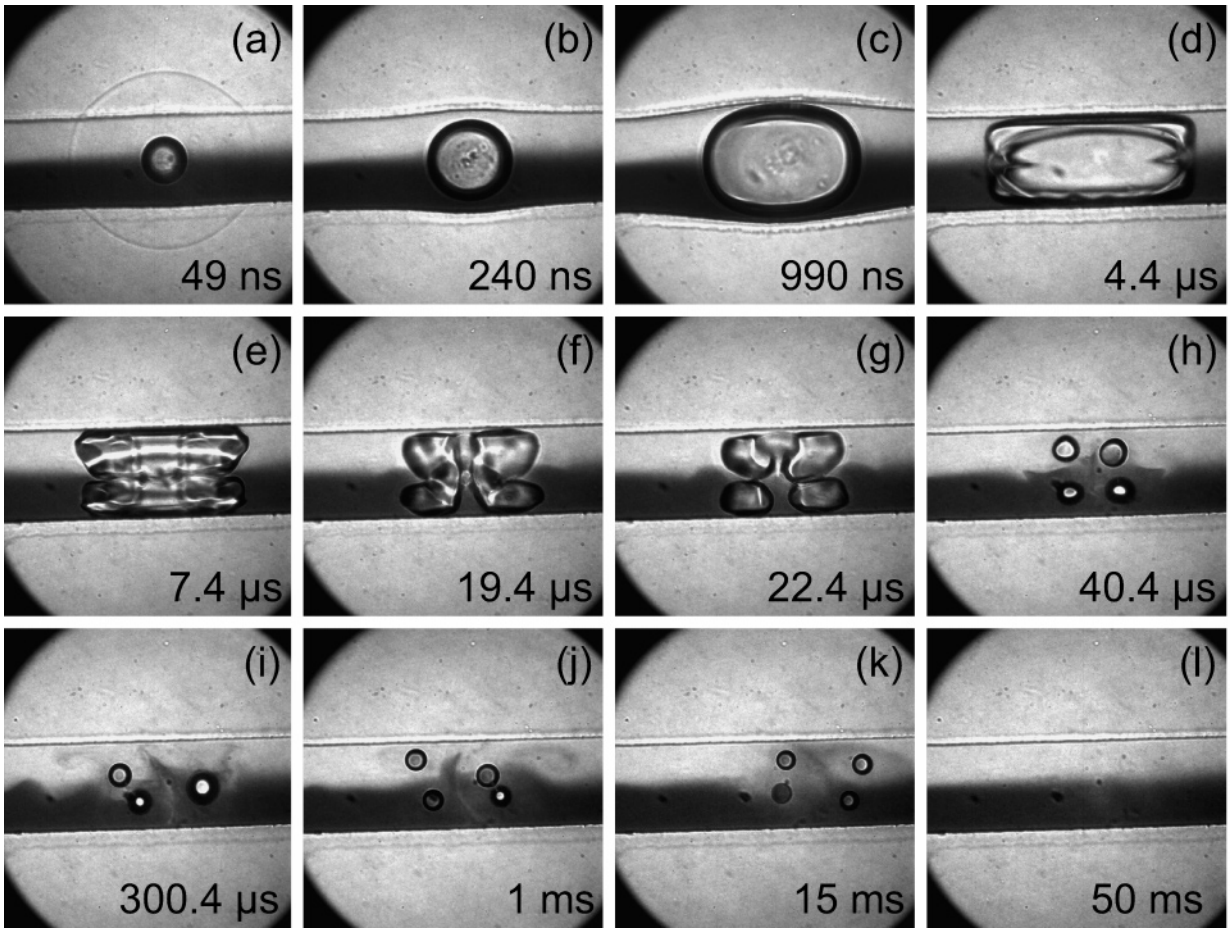

Figure 4. Time-resolved image series for cavitation bubble dynamics and mixing within a 100-μm-wide microfluidic channel.

The ellipsoidal bubble reaches a maximum "length" of 240 μm (measured along its longest axis) at a time of 4.4 μs. The maximum volume of the cavitation bubble is estimated as 1.04 nL, which corresponds to the volume of an ellipsoid with dimensions of 240, 165, and 50 μm along its three axes.

After reaching its maximum size, the bubble collapses rapidly with the reduction in the bubble size occurring faster in the direction parallel with the channel walls. The rapid fluid inflow associated with the bubble collapse results in bubble splitting along the longitudinal axis of the microchannel (Figure 3d,e) and produces counterpropagating jets toward the channel walls (Figures 3f−h). These jets produce a second bubble splitting event and the formation of four very small bubbles that are convected downstream. The appearance of the second bubble splitting event suggests that these jets occupy the full height of the microfluidic channel. These complex bubble dynamics disrupt the smooth interface separating the two fluids and mix the adjacent fluid streams. Upon bubble collapse, mixing is most evident in the upper part of the channel due to a higher concentration of Naphthol Green (Figure 3h,i). However, since the bubble collapse is symmetric relative to the interface that initially separates the two fluid streams, one can deduce that the mixing region is also symmetric. At 300 μs, we observe the generation of symmetrical whorls that are formed as a result of the impact of the fluid jet on the channel walls. The spatiotemporal dynamics of the mixing process are remarkably reproducible, demonstrating that laser-generated cavitation bubbles produce consistent well-defined fluid patterns upon collapse within a microfluidic channel. In this case, the mixing zone has a lateral extent of roughly 250 μm that persists for ~50 ms, after which restoration of the interface between the two adjacent fluids begins and the region of mixed fluid flows downstream and out of the field of view. Since we image the dynamics in one plane, the total volume in which this fluid jetting and mixing occurs is unknown. However, by approximating the mixed region as an ellipsoid with dimensions equal to 250 μm × 200 μm × 50 μm, we can estimate the mixed volume of fluid to be 1.3 nL.

Figure 4 shows the mixing dynamics within a 100-μm-wide channel using a laser pulse energy of 25 μJ. The ellipsoidal bubble shape is even more elongated due to the smaller channel cross section and reaches a maximum length of 230 μm (Figure 4d). The stronger confinement offered by the smaller channel reduces the maximum bubble volume even more than that seen in Figure 3 even though a higher pulse energy was used to cause plasma formation. Using measured dimensions of 230 μm × 110 μm × 50 μm, we calculate a maximum ellipsoidal bubble volume of only 0.6 nL. Another interesting feature is the transient deformation of the channel walls caused by the rapid bubble expansion as seen in Figure 4c.

The features of the bubble collapse are slightly different from those seen in Figure 3. The narrower channel enhances the speed of the bubble collapse along the longitudinal axis of the channel that again results in complete bubble splitting upon collapse (Figure 4e,f). Again, we see counterpropagating jets toward the

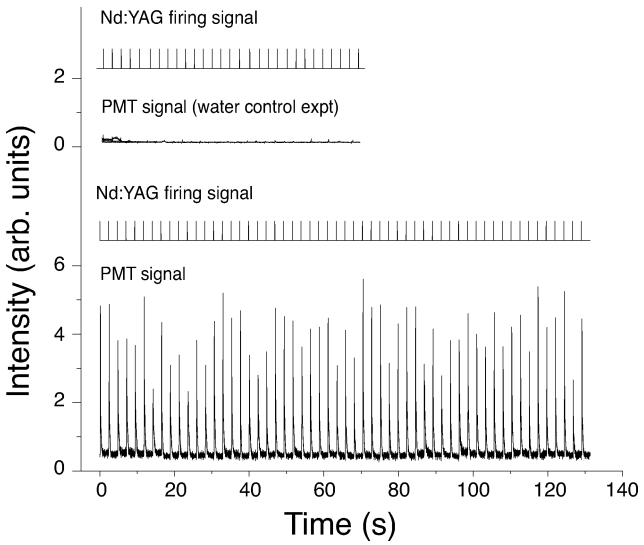

Figure 5. Fluorescent detection of mixing effects produced by Nd:YAG laser pulses using the setup shown in Figure 2.

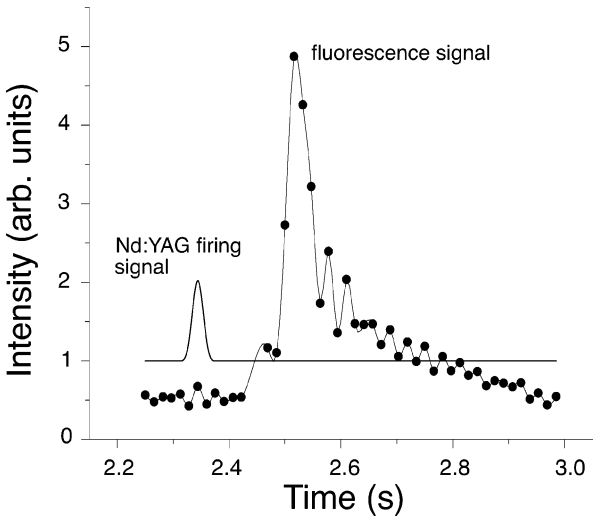

Figure 6. Expanded view of one fluorescence signal peak from Figure 5 with the corresponding Nd:YAG firing signal.

bubble walls that occupy the full height of the microfluidic channel and result in the second bubble splitting event. The jets produced in the 100-μm-wide channel seem to produce more lateral mixing upon bubble collapse (Figure 4h−k) than in the 200-μm-wide channel. In this case, the mixed region extends laterally for a distance of 200 μm and persists until the interface is restored at 50 ms. Again we see that while the bubble collapse is complete within 50 μs, the mixing dynamics persist for more than 15 ms. Approximating the mixed fluid region by an ellipsoid with dimensions 200 μm × 100 μm × 50 μm provides an estimate of 0.52 nL for the mixed fluid volume.

Downstream Fluorescence Detection of Mixed Bolus of Water and Fluorescein. The PMT-based fluorescence detection system was employed to examine the characteristics of the mixed bolus of fluid roughly 7 mm downstream from the region where the Nd:YAG laser pulse was delivered. The focal volume of the argon ion laser output used to excite fluorescence was placed at a lateral position in the microfluidic channel where only water was present so long as the parallel laminar flow of the water and fluorescein solution remained undisturbed. Figure 5 shows the result of one experimental run using this system. The first pair of traces shown in Figure 5 provide signals for the firing of the Nd:YAG laser used to produce the mixing and the measured signal from the PMT when water was supplied to both inlets of the microfluidic device. This shows that the presence of only water in the channel results in no significant PMT signal even when mixing is produced upstream by the firing of the Nd:YAG laser. The second pair of traces show results when one of the water streams is replaced by a 10 μM fluorescein solution. The firing of each Nd:YAG laser pulse results in a spike in the PMT signal indicating the presence of the fluorescein solution on the side of the microfluidic channel where only water is usually present. This result is indicative of the production of a mixed bolus of fluid that occupies nearly the entire width of the channel and is convected down the channel along with the main flow. Some pulse-to-pulse variation in the peak intensity of the fluorescence signal measured by the PMT is observed. This variation is likely due to the small fluid volume interrogated by the confocal fluorescence detection system and the 60-Hz sampling rate of the PMT signal, which may be insufficient to adequately resolve the temporal fluctuations in fluorescent intensity on the microscale.

Figure 6 provides an expanded plot of one fluorescence signal peak from Figure 5 that follows the firing signal produced by the Nd:YAG laser. The delay of 120 ms between the Nd:YAG firing signal and the increase in the fluorescence signal is not meaningful as it takes several seconds for the bolus of mixed fluid to travel the several millimeters between the site of mixing and the site of fluorescence detection. Thus, the fluorescence intensity peak that is detected due to fluid mixing is not produced by the Nd:YAG laser pulse whose firing signal is shown, but by a preceding laser pulse. The width of the fluorescent peak (measured full width at half-maximum) is 70 ms. This indicates that the bulk of the detected fluorescein is concentrated in a bolus of mixed fluid ~200 μm in length for the total volumetric flow rate of 100 μL/h in the 200 μm × 50 μm microfluidic channel. This dimension is roughly consistent with the dimensions of the mixed bolus of fluid visualized in our time-resolved imaging experiments. Close examination of the PMT signal immediately surrounding the main peak reveals a "ringing" pattern. This may indicate that a small region is present between the main bolus of mixed fluid and unmixed fluid where there are larger scale fluid structures of fluorescein and water. In this experiment, a Nd:YAG laser pulse repetition rate of 0.4 Hz was chosen in order to create a small region of mixed fluid followed by an unmixed region. The duration of the fluorescence peak suggests that continuous mixing within the channel can be achieved by increasing the pulse repetition rate of the Nd:YAG laser to 6−10 Hz.

Fluorescence Imaging of Amplex Red/HRP Reaction. To demonstrate that the laser-induced mixing observed in the time-resolved imaging studies is sufficient to initiate a biochemical reaction within a continuous-flow microfluidic system, we used this technique to initiate the HRP-catalyzed reaction between H_2O_2 and Amplex Red. In the presence of HRP, Amplex Red reacts with H_2O_2 in a 1:1 stoichiometry, producing highly fluorescent resorufin.[34] Figure 7a is a bright-field image at the intersection merging

(34) Zhou, M. J.; Diwu, Z. J.; Panchuk-Voloshina, N.; Haugland, R. P. *Anal. Chem.* **2004**, *76*, 3694−3698.

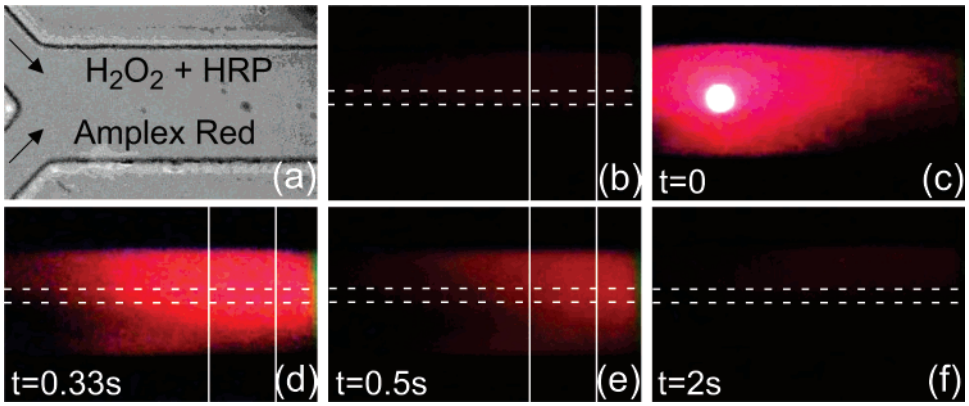

Figure 7. Image series demonstrating the production of fluorescent resorufin using the proposed mixing technique to initiate the HRP-catalyzed reaction between Amplex Red and hydrogen peroxide.

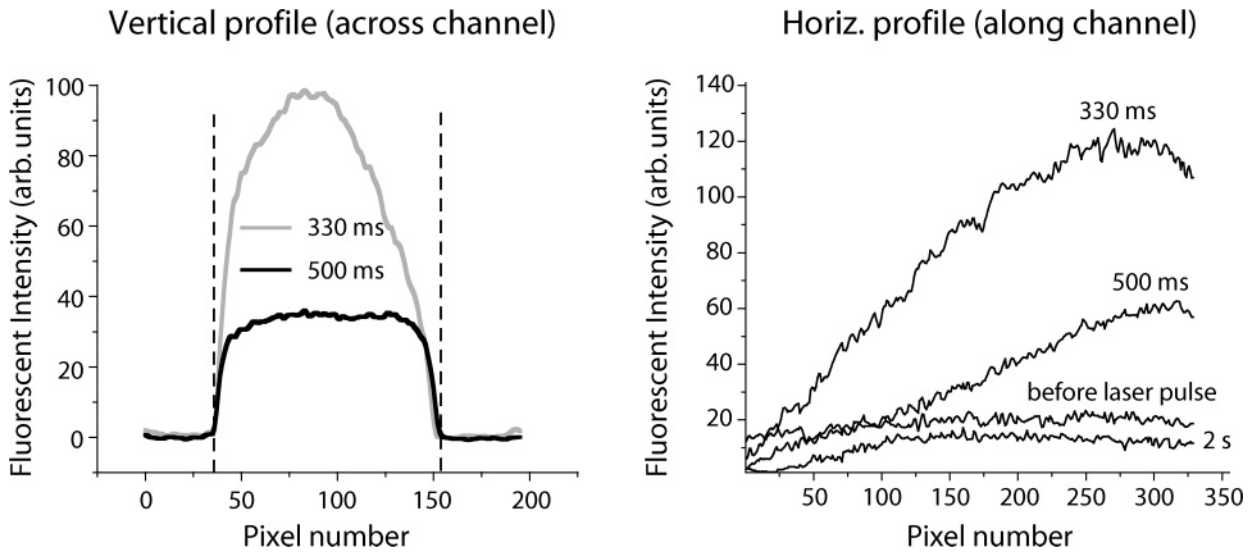

Figure 8. Quantitative analysis of the fluorescent images in Figure 7 demonstrating that the fluorescent product resorufin is produced throughout the entire width of the microfluidic channel and is convected downstream with the main hydrodynamic flow.

the two nonfluorescent streams: H_2O_2 and HRP in the top stream and Amplex Red in the bottom stream. Figure 7b provides a "background" fluorescence image prior to delivery of the laser pulse. Figure 7c provides the fluorescence image at the time of laser pulse delivery ($t = 0$) showing the fluorescence produced by the plasma emission. Panels d and e in Figure 7 are fluorescence images taken $t = 0.33$ and 0.5 s following the laser pulse delivery, respectively. One can easily identify a "bolus" of fluorescence that corresponds to the formation of the reaction product that occupies the entire width of the channel and is convected downstream by the main flow. Figure 7f is the fluorescence image at $t = 2$ s following the laser pulse delivery and bears a strong similarity to Figure 7b since the bolus of the fluorescent reaction product has been convected downstream and out of the field of view. This time scale for the flow of the reaction product out of the field of view and the re-establishment of parallel laminar flow is consistent with the mean flow velocity of 560 μm/s.

To provide a more quantitative assessment of the spatial distribution of the fluorescent reaction product within the channel, we provide the spatial distribution of the fluorescent intensities in Figure 8. Figure 8a is an integrated measure of the fluorescent intensity as a function of *vertical* position within the channel between the two vertical solid lines shown in Figure 7b, d, and e. The fluorescent intensities shown are those determined from Figure 7d and e normalized against the "background" intensity of Figure 7b. These traces clearly show that the fluorescent product of the reaction occupies the full width of the channel. Figure 8b is an integrated measure of the fluorescent intensity as a function of *horizontal* position along the length of the channel between the two horizontal dashed lines shown in Figure 7b and d−f. This figure illustrates the minimal fluorescence intensity before and 2 s following the laser delivery as well as the propagation of the reaction product downstream on the subsecond time scale.

DISCUSSION

These time-resolved imaging and fluorescence methods have enabled the examination of both the hydrodynamic events that lead to the formation of a small volume of mixed fluid and its downstream convection in the microfluidic channel on nanosecond to second time scales. The initiating event for the mixing process is the formation of a laser-induced plasma within the aqueous medium. Plasma formation is a nonlinear process and does not rely on linear optical absorption by the aqueous medium. Thus, the proposed method is applicable at any optically accessible

location within a microfluid device. The process of laser-induced plasma formation in water is a well-studied phenomenon whose lifetime, for nanosecond pulse widths, is governed by the duration of the laser pulse.[32] The rapid plasma expansion results in cavitation bubble formation, expansion, and collapse; processes that are all clearly visualized within the microfluidic channel. The confinement offered by the microfluidic channel results in maximum bubble volumes that are smaller than those observed for expansion in a free medium. The confinement also results in bubble splitting and jet formation upon bubble collapse that accomplishes the fluid mixing. While cavitation bubble dynamics in the proximity of single rigid or elastic boundaries[35,36] as well as bubble−bubble interactions within microfluidic channels[37] have been studied, we believe this is the first examination of the dynamics of a single cavitation bubble within a channel whose dimensions are similar in size to the bubble itself. The hydrodynamic resistance offered by the microfluidic channel walls results in the more rapid collapse of the bubble surfaces that are not adjacent to the channel walls. This leads to asymmetric bubble collapse, specifically invagination or "pinching" of the bubble wall in the midplane of the channel, followed by jet formation and a second bubble splitting event. While the impact of cavitation-induced jets have been known to cause pitting damage in metal films and tissue puncture in ophthalmic surgery,[38] we do not observe mechanical damage due to the low laser pulse energies used and the mechanical resiliency of PDMS. Instead, upon hitting the channel walls, the jet flows outward, leading either to whorl formation in the case of the 200-μm channel or more complex patterns seen in the case of the 100-μm channel. The bubble collapse dynamics also caused stretching and folding of fluid elements, characteristics necessary for good micromixing. We also observed that the mixing region extended to regions upstream of the flow leading to "active mixing", defined as a process in which the fluid interfaces interact with the flow and modify it.[39] Clearly, the imaging system employed here could find general use for the examination and analysis of other fast biophysical effects in microfluidic devices.[40]

Although mixers based on the use of ultrasound to generate cavitation bubbles have been described,[21,22,41] there are several important differences between our method and those that employ ultrasound. In ultrasonic mixers, an acoustic wave is launched into the medium by a piezoelectric transducer that is integrated onto the device. Mixing occurs due to microflows and eddies set up by cavitation microstreaming. In our method, the localized flow instability and mixing is produced by a single bubble, as opposed to the formation of multiple bubbles as is the case for cavitation microstreaming. The site of bubble formation (and hence mixing) can be accurately controlled by focusing the laser microbeam with a high numerical aperture objective at the desired location. The bubble collapse was found to produce flow patterns that were reproducible on both microsecond and millisecond time scales. Since flow patterns produced during ultrasound mixing in microchannels have not been studied, it is not known whether similar processes are operative in these methods.

The production of cavitation bubble-induced mixing through laser-induced plasma formation may be cause for concern due to the potential for direct damage by the plasma. While the plasma itself can reach high temperatures,[42] the plasma is typically very small (~10-μm diameter), has a short lifetime (~20 ns), and cools rapidly upon expansion. Nonetheless, it is likely that an amount of fluid equivalent to the plasma volume is thermally inactivated. Experimental studies show that, for the laser parameters used in this study, the plasma volume is well-described by an ellipsoid ~13 μm in length and ~8 μm in diameter resulting in a plasma volume of ~0.7 pl.[31,43] This suggests that there is over a 1000:1 ratio between the volume of mixed fluid (~1 nL) to the volume of reactants destroyed by plasma formation. Moreover, even if the entire energy of the 20-μJ laser pulse is confined to the mixed fluid volume on the order of 1 nL, the resulting temperature rise is no more than 5 deg kelvin. Our successful demonstration of the HRP-catalyzed reaction of Amplex Red and H_2O_2 resulting in resorufin demonstrates that any generated heat did not result in significant inactivation of the reactants, catalyst, or product. One potential limitation of this technique is that the plasma does indeed vaporize a small volume of fluid thereby leading to the generation of vapor bubbles that persist after the cavitation bubble collapse. Although we did not encounter problems when operating the Nd:YAG laser at a pulse repetition rate of 0.4 Hz, higher pulse repetition rates may lead to the generation of large numbers of vapor bubbles that could block the channel. This can be remedied by the use of shorter wavelengths (e.g., $\lambda = 355$ nm) or shorter laser pulse durations (ps or fs).[44,45] Reductions in wavelength or pulse duration enable the formation of a laser-induced plasma at lower pulse energies (≤ 1 μJ/pulse) with less energy available for vaporization. However, this may also lead to a smaller amount of bubble energy, leading to less violent bubble collapse and the production of smaller volumes of mixed fluid. Another approach could be surface modification of the channel walls to make them more hydrophilic and less prone to bubble sticking. Clearly the promising results of this study need to be followed up with a detailed examination of the dependence of the fluid mixing process on laser pulse duration, pulse energy, wavelength, and pulse repetition rate.

CONCLUSION

We have demonstrated a novel technique for mixing two streams within a microfluidic channel using laser-generated cavitation bubbles. Time-resolved imaging allowed visualization of the complex fluid patterns produced upon bubble collapse. While the cavitation bubble formation expansion and collapse was

(35) Vogel, A.; Lauterborn, W.; Timm, R. *J. Fluid Mech.* **1989**, *206*, 299−338.
(36) Brujan, E. A.; Nahen, K.; Schmidt, P.; Vogel, A. *J. Fluid Mech.* **2001**, *433*, 251−281.
(37) Chen, Y. H.; Chu, H. Y.; I, L. *Phys. Rev. Lett.* **2006**, *96*, 034505.
(38) Vogel, A.; Schweiger, P.; Frieser, A.; Asiyo, M. N.; Birngruber, R. *IEEE J. Quantum Electron.* **1990**, *26*, 2240−2260.
(39) Ottino, J. *The kinematics of mixing: stretching, chaos and transport*; Cambridge Texts in Applied Mathematics; Cambridge University Press: Cambridge, UK, 1988.
(40) Grumann, M.; Brenner, T.; Beer, C.; Zengerle, R.; Ducrée, J. *Rev. Sci. Instrum.* **2005**, *76*, 025101.
(41) Liu, R. H.; Lenigk, R.; Druyor-Sanchez, R. L.; Yang, J.; Grodzinski, P. *Anal. Chem.* **2003**, *75*, 1911−1917.
(42) Stolarski, D. J.; Hardman, J.; Bramlette, C. M.; Noojin, G. D.; Thomas, T. J.; Rockwell, B. A.; Roach, W. P. *Proc. SPIE* **1995**, *2391*, 100−109.
(43) Colombelli, J.; Grill, S. W.; Stelzer, E. H. K. *Rev. Sci. Instrum.* **2004**, *75*, 472−479.
(44) Vogel, A.; Noack, J.; Nahen, K.; Theisen, D.; Busch, S.; Parlitz, U.; Hammer, D. X.; Noojin, G. D.; Rockwell, B. A.; Birngruber, R. *Appl. Phys. B* **1999**, *68*, 271−280.
(45) Vogel, A.; Venugopalan, V. *Chem. Rev.* **2003**, *103*, 577−644.

complete on a time scale of ~25 μs, the restoration of laminar flow did not occur until 50 ms following the laser pulse delivery. The cavitation bubble dynamics disrupted the parallel laminar flow and led to the formation of a local volume of mixed fluid. We estimated this mixed volume to be in the range of 0.5−1.5 nL. Fluorescence detection downstream of the mixing site confirmed that the delivery of each Nd:YAG laser pulse resulted in the formation of a mixed bolus of fluid that occupied the entire channel and was convected downstream with the main flow. We also used fluorescence video microscopy to demonstrate that laser-induced mixing can be used to initiate an enzyme-catalyzed reaction within a microfluidic system. This method of mixing using laser-generated cavitation bubbles may be particularly attractive for microfluidic applications since no modifications need be made to the microfluidic channel geometry and there is complete flexibility in the location of the mixing site. Moreover, the time-resolved imaging system detailed in this report could be used for the visualization of other fast phenomena in microfluidics.

ACKNOWLEDGMENT

We thank Prof. Mark Bachman for helpful discussions. We are grateful to the NIH for support under Grant R01-EB04436 and the Laser Microbeam and Medical Program (#P41-RR01192). Support is also provided by the University of California System-wide Biotechnology Research and Education Program (UC BREP) GREAT Training Grant #2006-12.

Received for review January 12, 2007. Accepted April 6, 2007.

AC070081I